been described for the present day[26] and the mid-Holocene[27].

Coupled Sr/Ca and $\delta^{18}O$ analyses at biannual and monthly resolution on the YD *Diploastrea* permit us to derive information about the coupled ocean–atmosphere response to YD cooling indicated by changes in the balance of evaporation and precipitation (Figs 2 and 3). When the relative contributions of SST and changes in $\delta^{18}O_{SW}$ to the coral $\delta^{18}O$ record are deconvolved[24,25], we find that $\delta^{18}O_{SW}$ tracks SST variability. Although the error on the reconstructed $\delta^{18}O_{SW}$ is large because it includes errors in both the Sr/Ca and $\delta^{18}O$ methods[25], the main variations in $\delta^{18}O_{SW}$ are robust features of the record. Positive correlation between SST and $\delta^{18}O_{SW}$ is evident on both interdecadal (Fig. 2) and seasonal (Fig. 3) timescales.

In the modern tropical western Pacific Ocean, $\delta^{18}O_{SW}$ is positively correlated with sea surface salinity (SSS)[28], in large part owing to seasonal differences in the amount of ^{18}O-depleted precipitation. At Vanuatu today, both $\delta^{18}O_{SW}$ and SSS decrease as SST rises during the austral summer intensification of the South Pacific convergence zone (SPCZ), which brings greater in-mixing of ^{18}O-depleted precipitation. This contrasts with the subtropical southwestern Pacific, where modern coral reconstructions and instrumental records from areas not affected by moisture transport into the SPCZ demonstrate that SST and SSS are positively correlated[24,25]. Therefore, in subtropical oceanic settings where evaporation strongly exceeds precipitation, as SST increases, so do $\delta^{18}O_{SW}$ and SSS. This situation is the same as that encountered at Vanuatu during the YD, but opposite to that found today. Given the apparent compression of the tropics towards the Equator during the YD, the positive coupling between SST and $\delta^{18}O_{SW}$ in the *Diploastrea* record strongly suggests that the SPCZ did not exist during this period. A partial analogue for the YD climate scenario is provided by modern El Niño events, when the Western Pacific warm pool contracts towards the Equator and the SPCZ migrates northwards to merge with the inter-tropical convergence zone.

It is beyond the scope of the present study to determine the potential mechanisms for the strong interdecadal variability during the YD documented by the *Diploastrea* record. Although recent modelling studies[29,30] indicate that interdecadal variability in the tropical Pacific can be generated solely by tropical wind forcing, most theories invoke links to the mid-latitudes. Clearly, more high-resolution palaeoclimate records from low to high latitudes, and further modelling studies, are needed to fully understand the ocean–atmosphere processes driving the altered YD climatic regime. □

Received 28 October 2003; accepted 16 March 2004; doi:10.1038/nature02506.

1. Peteet, D. Global Younger Dryas? *Quat. Int.* **28,** 93–104 (1995).
2. Anderson, D. Younger Dryas research and its implications for understanding abrupt climatic change. *Prog. Phys. Geogr.* **21,** 230–249 (1997).
3. Watanabe, O. *et al.* Homogeneous climate variability across East Antarctica over the past three glacial cycles. *Nature* **422,** 509–512 (2003).
4. Bennett, K. D., Haberle, S. G. & Lumley, S. H. The last Glacial-Holocene transition in southern Chile. *Science* **290,** 325–328 (2000).
5. Singer, C., Shulmeister, J. & McLea, B. Evidence against a significant Younger Dryas cooling event in New Zealand. *Science* **281,** 812–814 (1998).
6. Rodbell, D. T. & Seltzer, G. O. Rapid ice margin fluctuations during the Younger Dryas in the Tropical Andes. *Quat. Res.* **54,** 328–338 (2000).
7. Thompson, L. G. Ice core evidence for climate change in the tropics: implications for our future. *Quat. Sci. Rev.* **19,** 19–35 (2000).
8. Guilderson, T. P., Fairbanks, R. G. & Rubenstone, J. L. Tropical Atlantic coral oxygen isotopes: glacial-interglacial sea surface temperatures and climate change. *Mar. Geol.* **172,** 75–89 (2001).
9. Ruhlemann, C., Mulitza, S., Muller, P. J., Wefer, G. & Zahn, R. Warming of the tropical Atlantic Ocean and slowdown of thermohaline circulation during the last deglaciation. *Nature* **402,** 511–514 (1999).
10. Koutavas, A., Lynch-Stieglitz, J., Marchitto, T. M. & Sachs, J. P. El Niño-like pattern in ice age tropical Pacific sea surface temperature. *Science* **297,** 226–230 (2002).
11. Kienast, M., Steinke, S., Stattegger, K. & Calvert, S. E. Synchronous tropical south China sea SST change and Greenland warming during deglaciation. *Science* **291,** 2132–2134 (2001).
12. Thunell, R. C. & Miao, Q. Sea surface temperature of the western equatorial Pacific Ocean during the Younger Dryas. *Quat. Res.* **46,** 72–77 (1996).
13. Stott, L., Poulsen, C., Lund, S. & Thunell, R. Super ENSO and global climate oscillations at millennial time scales. *Science* **297,** 222–226 (2002).
14. Beck, J. W. *et al.* Sea-surface temperature from coral skeletal strontium/calcium ratios. *Science* **257,** 644–647 (1992).
15. Patrick, A. & Thunell, R. C. Tropical Pacific sea surface temperatures and upper water column thermal structure during the last glacial maximum. *Paleoceanography* **12,** 649–657 (1997).
16. Andres, M. S., Bernasconi, S. M., McKenzie, J. A. & Röhl, U. Southern Ocean deglacial record supports global Younger Dryas. *Earth Planet. Sci. Lett.* **216,** 515–524 (2003).
17. Cabioch, G. *et al.* in *Reefs and Carbonate Platforms in the Pacific and Indian Oceans* (eds Camoin, G. & Davies, P. J.) 261–277 (IAS Special Publication Vol. 25, International Association of Sedimentologists, Blackwell, Oxford, 1998).
18. Burr, G. S. *et al.* A high resolution radiocarbon calibration between 11,700 and 12,400 calendar years BP derived from ^{230}Th ages of corals from Espiritu Santo Island, Vanuatu. *Radiocarbon* **40,** 1093–1105 (1998).
19. Watanabe, T., Gagan, M. K., Corrège, T., Scott-Gagan, H. & Hantoro, W. S. Oxygen isotopes systematics in *Diploastrea heliopora*: New coral archive of tropical paleoclimate. *Geochim. Cosmochim. Acta* **67,** 1349–1358 (2003).
20. McConnaughey, T. ^{13}C and ^{18}O isotopic disequilibrium in biological carbonates: I. Patterns. *Geochim. Cosmochim. Acta* **53,** 151–162 (1989).
21. Gagan, M. K., Chivas, A. R. & Isdale, P. J. High-resolution isotopic records from corals using ocean temperature and mass-spawning chronometers. *Earth Planet. Sci. Lett.* **121,** 549–558 (1994).
22. Stoll, H. M. & Schrag, D. P. Effects of Quaternary sea level cycles on strontium in seawater. *Geochim. Cosmochim. Acta* **62,** 1107–1118 (1998).
23. Fairbanks, R. G. A 17,000-year glacio-eustatic sea level record: Influence of glacial melting rates on the Younger Dryas event and deep-ocean circulation. *Nature* **342,** 637–642 (1989).
24. Gagan, M. K. *et al.* Temperature and surface-ocean water balance of the mid-Holocene tropical western Pacific. *Science* **279,** 1014–1018 (1998).
25. Ren, L., Linsley, B. K., Wellington, G. M., Schrag, D. P. & Hoegh-Guldberg, O. Deconvolving the $\delta^{18}O$ seawater component from subseasonal coral $\delta^{18}O$ and Sr/Ca at Rarotonga in the southwestern subtropical Pacific for the period 1726 to 1997. *Geochim. Cosmochim. Acta* **67,** 1609–1621 (2003).
26. Delcroix, T. & Hénin, C. Mechanisms of subsurface thermal structure and sea surface thermohaline variabilities in the southwestern tropical Pacific during 1979–85. *J. Mar. Res.* **47,** 777–812 (1989).
27. Corrège, T. *et al.* Evidence for stronger El Niño Southern Oscillation (ENSO) events in a mid-Holocene massive coral. *Paleoceanography* **15,** 465–470 (2000).
28. Schmidt, G. A. Error analysis of paleosalinity calculations. *Paleoceanography* **14,** 422–429 (1999).
29. An, S. I. & Wang, B. Interdecadal change of the structure of the ENSO mode and its impact on the ENSO frequency. *J. Clim.* **13,** 2044–2055 (2000).
30. Karspeck, A. R. & Cane, M. A. Tropical Pacific 1976–77 climate shift in a linear, wind-driven model. *J. Phys. Oceanogr.* **32,** 2350–2360 (2002).

Supplementary Information accompanies the paper on **www.nature.com/nature**.

Acknowledgements We thank A. Ganachaud and the participants of the 'International workshop on the low frequency modulation of ENSO' (Toulouse, September 2003) for discussions and comments; H. Scott-Gagan for help with the isotopic measurements; Y. Join, J. L. Laurent, M. Lardy, F. Taylor and J. Récy for providing assistance in the field; the government of Vanuatu for allowing us to drill in Espiritu Santo; and B. Suwargadi, S. Fallon, D. Whitford, G. Whitford and the Indonesian Institute of Sciences (LIPI) for support with coral drilling in Alor, Indonesia. The IRD, ANU and NSF supported this work.

Competing interests statement The authors declare that they have no competing financial interests.

Correspondence and requests for materials should be addressed to T.C. (thierry.correge@noumea.ird.nc). Coral data presented here are available at http://www.ngdc.noaa.gov/paleo/coral/vanuatu.html.

Polysaccharide aggregation as a potential sink of marine dissolved organic carbon

Anja Engel[1]*, Silke Thoms[1], Ulf Riebesell[1]*, Emma Rochelle-Newall[2]* & Ingrid Zondervan[1]

[1]*Alfred-Wegener-Institut für Polar- und Meeresforschung, 27515 Bremerhaven, Germany*
[2]*Laboratoire d'Océanographie de Villefranche sur Mer, Station Zoologique, B.P. 28, F-06234 Villefranche-sur-Mer, France*

* Present addresses: Marine Sciences Research Center, Stony Brook University, Stony Brook, New York 11794-5000, USA (A.E.); Leibniz-Institut für Meereswissenschaften, Universität Kiel, 24105 Kiel, Germany (U.R.); Centre IRD de Noumea, BPA5, 98848 Noumea, New Caledonia (E.R.-N.)

The formation and sinking of biogenic particles mediate vertical mass fluxes and drive elemental cycling in the ocean[1]. Whereas marine sciences have focused primarily on particle production by phytoplankton growth, particle formation by the assembly of organic macromolecules has almost been neglected[2,3]. Here we

show, by means of a combined experimental and modelling study, that the formation of polysaccharide particles is an important pathway to convert dissolved into particulate organic carbon during phytoplankton blooms, and can be described in terms of aggregation kinetics. Our findings suggest that aggregation processes in the ocean cascade from the molecular scale up to the size of fast-settling particles, and give new insights into the cycling and export of biogeochemical key elements such as carbon, iron and thorium.

Marine biogeochemists operationally divide substances into particulate and dissolved matter, as their cycling and fate are functionally different: whereas particles can sink gravitationally and thereby transport matter between the surface and the deeper ocean, solutes remain in the water they are produced in. Most organic particles suspended in sea water are microscopically identifiable as plankton organisms or their debris. Thus, the concept of the biological carbon pump was originally developed around cell growth as the sole source of particulate organic matter (POM)[4]. In consequence, carbon export out of the sunlit surface ocean was hypothesized to be related to the amount of nutrients that can sustain the planktonic 'new production'[5,6].

Not all organic particles in the ocean originate from cell growth. Recently, extracellular polysaccharide particles, described as transparent exopolymeric particles (TEP), gained much attention in marine and freshwater science[7]. Owing to their surface-reactive nature, TEP support coagulation processes and enhance the formation of large particle aggregates (marine snow)[7,8], which in turn accelerate carbon export to the deep sea[9]. Chin *et al.*[2] demonstrated that exopolymer particles, such as TEP, spontaneously form from filtered precursors (<0.2 μm) under laboratory conditions. The relevance of abiotic processes for the transformation of dissolved organic matter (DOM) into POM in a more natural environment and relative to the degradation of DOM by microorganisms has yet to be demonstrated.

To examine the role of solute–particle transformation for carbon cycling, we traced dissolved polysaccharides (PCHO) and TEP during a bloom experiment with *Emiliania huxleyi*, a marine calcifying phytoplankton species known to produce and release an acidic polysaccharide[10]. Samples were collected over a period of 16 days from nine enclosures (11 m^3 each, 4 m water depth) deployed in a Norwegian fjord. To ensure bloom development, each enclosure was enriched with nutrients to yield initial concentrations of 15 μmol l^{-1} nitrate and 0.5 μmol l^{-1} phosphate and was gently mixed throughout the study by means of an airlift. Biomass accumulation was detectable after day 5 (Fig. 1a) and led to phosphate and nitrate depletion after days 11 and 13, respectively[11]. PCHO accumulated fast during the bloom, reached a maximum concentration of 20 μmol C l^{-1} at day 11 and decreased rapidly

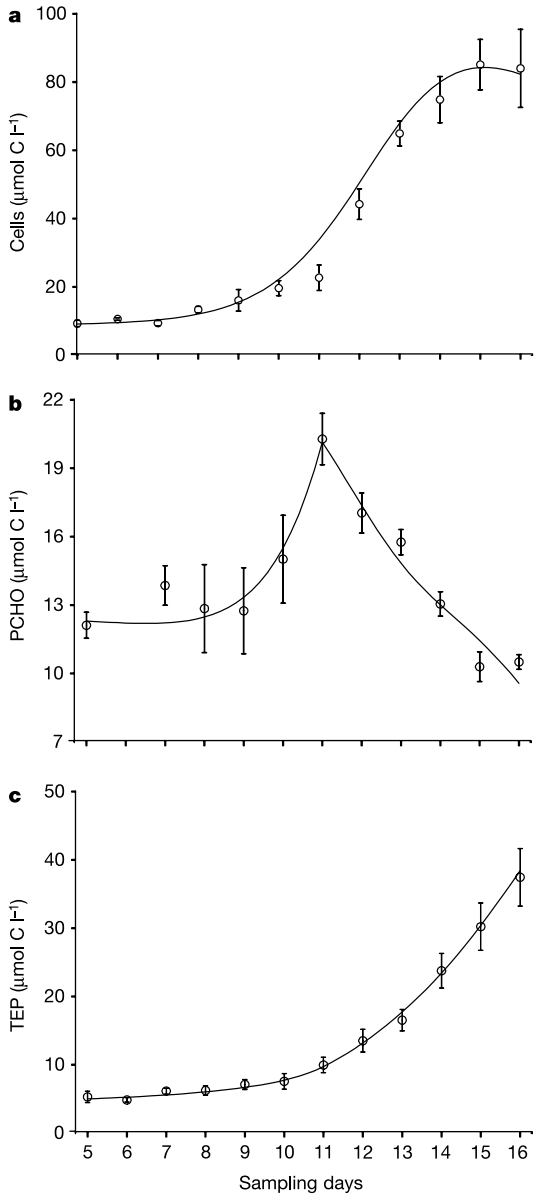

Figure 1 Observed and modelled dynamics of organic carbon during a mesocosm bloom experiment with the marine phytoplankton species *Emiliania huxleyi*. **a**–**c**, Depicted is organic carbon contained in algal cells (**a**), dissolved polysaccharides (PCHO; **b**) and transparent exopolymer particles (TEP; **c**). Symbols represent average values of nine mesocosms. Error bars denote one standard deviation. The solid lines represent the model results.

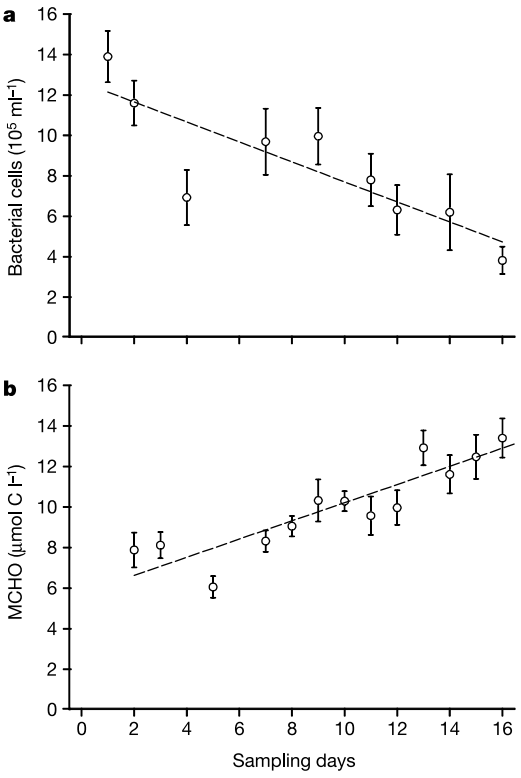

Figure 2 Observed dynamics of bacteria and mono- and oligosaccharides. **a**, **b**, The decrease of bacterial abundance during the bloom (**a**) coincided with an accumulation of dissolved mono- and oligosaccharides (MCHO; **b**). Symbols represent average values of six mesocosms in **a** and nine in **b**. Error bars denote one standard deviation. The dashed lines were calculated with a linear regression model I.

thereafter (Fig. 1b). The decrease of PCHO was tightly related to the increase of TEP concentration ($r^2 = 0.96$, $n = 54$, $P < 0.001$), which continued until the end of the study (Fig. 1c). The transfer of carbon from the dissolved to the particulate polysaccharide pool accounted for up to 30% of total particulate organic carbon (POC).

On the basis of the concept that two acidic polysaccharides approaching each other by diffusion can adhere, for example, through Ca^{2+} bridging, we hypothesize that the kinetics of carbon transfer from PCHO to TEP can be described in terms of cluster–cluster aggregation using Smoluchowski equations[12,13]. We tested this hypothesis with a two-size class, carbon-based model, which nevertheless retains the dominant properties of more complex aggregation models[14]:

$$\mathrm{d[PCHO]}/\mathrm{d}t = \gamma(MP_C - \mu)[\mathrm{cell}] - \alpha_{PCHO}\beta_{PCHO}[\mathrm{PCHO}]^2 - \alpha_{TEP}\beta_{TEP}[\mathrm{PCHO}][\mathrm{TEP}] \quad (1)$$

$$\mathrm{d[TEP]}/\mathrm{d}t = \alpha_{PCHO}\beta_{PCHO}[\mathrm{PCHO}]^2 + \alpha_{TEP}\beta_{TEP}[\mathrm{PCHO}] \times [\mathrm{TEP}] \quad (2)$$

Here, PCHO are represented as a fraction, γ, of the algal exudates, which are the photosynthetic assimilates not used for net growth $(MP_C - \mu)[\mathrm{cell}]$, with P_C being the carbon-specific photosynthetic rate and M a coefficient that allows for changes of P_C at the time of nutrient exhaustion[15]. The modelled extracellular release expressed as percentage of assimilated carbon varied from 21% initially to 77% at day 16, conforming with earlier findings[16]. The time-dependent cell growth rate, μ, was obtained by fitting the observed cellular carbon concentration, [cell], assuming [cell] = [POC] − [TEP], by a function that combines logistic growth with a loss term. The fit yielded a maximum growth rate of $0.8\,\mathrm{d}^{-1}$, which matches earlier measurements for *E. huxleyi*[17]. Because the contact rate between polysaccharides increases with abundance, the loss of carbon from PCHO and its gain in TEP are functions of their concentrations. The coefficient α determines the attachment probability after collision. The carbon-specific collision kernels, β, were estimated under the assumptions that the encounter rate of polysaccharides is controlled by diffusion (see equations (3) and (4) in Box 1) and that the primary units forming an aggregate are similar. The size of a new PCHO aggregate to represent a TEP is determined by the Heaviside step function, $\theta(x)$, included in β_{PCHO} (Box 1). Although simplifying the aggregation process, the model reproduced the carbon flow from PCHO to TEP, while maintaining all parameter values within previously observed ranges (Fig. 1a–c and Box Table 1). This suggests that PCHO–TEP dynamics can be described in terms of aggregation.

It has been assumed in marine science that degradation by heterotrophic bacteria is the primary process determining the fate of dissolved organic carbon (DOC) of high molecular mass[18], which is predominantly composed of polysaccharides[19]. However, for the *E. huxleyi* bloom it is unlikely that bacteria caused the observed decrease of PCHO, because limited bacterial activity was indicated by both a decrease in bacterial numbers over time ($r^2 = 0.72$, $n = 54$, $P < 0.001$) (Fig. 2a) and a continuous accumulation of mono- and oligosaccharides (MCHO) ($r^2 = 0.86$, $n = 144$, $P < 0.001$) (Fig. 2b), a preferred bacterial substrate that can be taken up without enzymatic processing. These findings are in accordance with earlier observations showing that PCHO released by *E. huxleyi* are resistant to bacterial degradation within a timescale of weeks[10]. Thus, at times of phytoplankton blooms, aggregation and sedimentation of PCHO may efficiently remove DOC from surface waters before bacteria can degrade it. Such a mechanism of DOC export could contribute to sustain the observed turnover of organic carbon in the mesopelagic ocean[20].

Our model results indicate that polysaccharide aggregation was driven mainly by PCHO–TEP interaction and that the decrease of PCHO was accelerated the more TEP were produced. This negative feedback explains why later during the bloom, newly released polysaccharides did not accumulate in the dissolved fraction, but were scavenged rapidly by the larger polysaccharide aggregates. Owing to their aggregate nature, TEP are fractal objects of large size relative to their mass. A rapid increase in TEP concentration therefore results in a sudden amplification of the total particulate volume in sea water. This in turn increases collision and coagulation rates with other suspended particles such as phytoplankton, eventually leading to marine snow formation and enhanced sedimentation rates.

A cascading aggregation mechanism such as the one proposed here can explain the short timescales that prevail when phytoplankton blooms flocculate and settle to the deeper ocean[9]. As the ultimate source of PCHO is phytoplankton exudation, a process that is thought to be regulated by a cell internal imbalance of CO_2 and nutrient assimilation, our findings indicate that marine snow formation, often in combination with mass sedimentation, is ultimately determined by the physiology of the phytoplankton.

Quantitatively, PCHO contribute between 5% and 40% to DOC concentration in the ocean[21]. They comprise a major fraction of phytoplankton exudates[22], and sometimes account for more than 50% of total primary production[23]. In coastal seas, PCHO easily reach concentrations similar to those observed during this experimental study[24]. At open ocean sites, carbon contained in PCHO generally exceeds POC concentration. Hence, PCHO may not only

Box 1
Parameter estimation

The values for the carbon-specific collision kernels β_{PCHO} and β_{TEP} were calculated as:

$$\beta_{PCHO} = \frac{1}{2TEP_0(0.4)^2}\int_0^{0.4}\int_0^{0.4}\left(\frac{1}{d_i^D}+\frac{1}{d_j^D}\right)K_b(d_i,d_j) \times \theta(d_i^D + d_j^D - 0.4^D)d(d_i)d(d_j) \quad (3)$$

$$= 0.86\,\mathrm{l\,\mu mol^{-1}\,d^{-1}}$$

$$\beta_{TEP} = \frac{1}{TEP_0 0.4(d_b - 0.4)}\int_0^{0.4}\int_{0.4}^{d_b}\frac{1}{d_j^D}K_b(d_i,d_j)d(d_i)d(d_j)$$

$$= 0.064\,\mathrm{l\,\mu mol^{-1}\,d^{-1}} \quad (4)$$

where D, the fractal dimension of polysaccharide aggregates, has a value of 2.55 (ref. 29); d_i and d_j are polysaccharide sizes; k, the Boltzmann constant, has a value of $1.38066 \times 10^{-23}\,\mathrm{J\,K^{-1}}$; $k_b(d_i, d_j)$, the coagulation kernel for brownian motion, is $\frac{2kT}{3\eta}\frac{(d_i+d_j)^2}{d_i d_j}$ (assuming that $d_i = d_j$ and $d_{h,i} = d_i$, with $d_{h,i}$ being the hydrodynamical diameter); TEP_0, the carbon content of a polysaccharide aggregate with 1-μm diameter, is $3.56 \times 10^{-9}\,\mu\mathrm{mol\,\mu m^{-D}}$; salinity is 30 psu (practical salinity units); T, temperature, is 283.15 K; η, viscosity, is $0.00138\,\mathrm{kg\,m^{-1}\,s^{-1}}$; d_b, the largest particle diameter for diffusion-dominated coagulation, is 8 μm (ref. 30); and $\theta(x)$, the Heaviside step function, is $\begin{cases}1, & x>0\\ 0, & \text{otherwise}\end{cases}$.

Box Table 1 **Parameter values**

Parameter	Symbol	Unit	Model values	Observed values
Attachment probability$_{(PCHO–PCHO)}$	α_{PCHO}	1	0.00087	≤0.001 (ref. 28)
Attachment probability$_{(PCHO–TEP)}$	α_{TEP}	1	0.4	0.1–1 (ref. 8)
PCHO exudation coefficient	γ	1	0.31 ($t < 11$); 0.13 ($t > 11$)	0.3–0.6 (ref. 22)
Maximum growth rate	μ_{max}	$\mathrm{d^{-1}}$	0.8	0.8 (ref. 17)
Nutrient acclimation coefficient	$M_{t<11}$	1	1	–
	$M_{t>11}$	1	0.39	0.1–0.3 (ref. 15)
Carbon-specific photosynthetic rate	P_C	$\mathrm{d^{-1}}$	1.8	1.8 (ref. 17)

regulate the timing of sedimentation processes, but through aggregation with sinking particles may also contribute directly to carbon export.

Recent advances in trace metal biogeochemistry have highlighted the importance of dissolved and colloidal organic matter for the cycling of trace nutrients such as Fe and Zn and of the particle reactive tracer ^{234}Th (ref. 25). Because polysaccharides provide strong binding sites for trace metals, aggregation and sedimentation of polysaccharides are key processes controlling trace metal residence times in the surface ocean. Implemented into larger ecosystem models, our findings could therefore help to reconcile observed dynamics in trace elements with carbon fluxes in the ocean.

Owing to their short-lived nature, the significance of dissolved polysaccharides in marine biogeochemical cycling has previously been overlooked. Whereas phytoplankton exudation has been considered to divert primary production from contributing to vertical flux, the mechanism described here constitutes an effective pathway to channel dissolved matter into the particulate pool. Because PCHO production is not constrained by nutrient supply, this pathway has the potential to modulate the stoichiometry of biogeochemical cycling in the ocean. Its relative contribution to overall primary production thereby strongly depends on the physiology of the phytoplankton and is likely to differ between species and as a function of environmental conditions. Global environmental change and the expected shift in phytoplankton composition are therefore bound to change the relative importance of this pathway, with likely consequences for carbon sequestration in the ocean. □

Methods

Determination of TEP, MCHO and PCHO

TEP were determined from 50–100-ml samples filtered onto Nuclepore filters (pore size of 0.4 μm)[26]. All filters were prepared in duplicates and stored at −20 °C until analysis. A carbon content of TEP of 39% (w/w) was determined[11] from 11 samples (5 l each) taken on different days.

MCHO and PCHO were determined after acidic hydrolysis (1 M HCl for 20 h at 100 °C) with the 2,4,6-tripyridyl-*s*-triazine (TPTZ) spectrophotometric method[24] from 30-ml samples, filtered through combusted GF/F filters into combusted glass vials and stored at −21 °C for less than 4 months. The carbon content of PCHO was calculated assuming a conversion of 30 μg glucose per μmol C.

Bacterial abundance

Bacterial abundance was determined at ×1,250 magnification using an epifluorescent microscope (Zeiss) and 4,6-diamidino-2-phenylindole (DAPI)-stained samples[27], preserved with 0.2-μm-filtered borax-buffered formalin (2% final concentration). Ten millilitres were stained with 0.2-μm-filtered DAPI solution for 10 min before filtering onto a black 0.2 μm Osmonics filter and stored at 4 °C. Bacterial abundance was estimated from 20–30 randomly selected fields per filter.

Received 24 October 2003; accepted 1 March 2004; doi:10.1038/nature02453.

1. Mc Cave, I. N. Vertical flux of particles in the ocean. *Deep-Sea Res.* **22,** 491–502 (1975).
2. Chin, W., Orellana, M. V. & Verdugo, P. Spontaneous assembly of marine dissolved organic matter into polymer gels. *Nature* **391,** 568–572 (1998).
3. Wells, M. L. A neglected dimension. *Nature* **391,** 530–531 (1998).
4. Volk, T. & Hoffert, M. I. in *The Carbon Cycle and Atmospheric CO_2; Natural Variations Archaen to Present* (eds Sundquist, E. T. & Broecker, W. S.) 99–110 (Geophys. Monogr. 32, American Geophysical Union, Washington DC, 1985).
5. Dugdale, R. C. & Goering, J. J. Uptake of new and regenerated forms of nitrogen in primary productivity. *Limnol. Oceanogr.* **12,** 196–206 (1967).
6. Eppley, R. W. & Peterson, B. J. Particulate organic matter flux and planktonic new production in the deep ocean. *Nature* **282,** 677–680 (1979).
7. Passow, U. Transparent exopolymer particles (TEP) in the marine environment. *Prog. Oceanogr.* **55,** 287–333 (2002).
8. Engel, A. The role of transparent exopolymer particles (TEP) in the increase in apparent particles stickiness (α) during the decline of a diatom bloom. *J. Plankton Res.* **22,** 485–497 (2000).
9. Asper, V. L., Deuser, W. G., Knauer, G. A. & Lorenz, S. E. Rapid coupling of sinking particle fluxes between surface and deep ocean waters. *Nature* **357,** 670–672 (1992).
10. Nanninga, H. J., Ringenaldus, P. & Westbroek, P. Immunological quantification of a polysaccharide formed by *Emiliania huxleyi*. *J. Mar. Syst.* **9,** 67–74 (1996).
11. Engel, A. *et al.* TEP and DOC production by *Emiliania huxleyi* exposed to different CO_2 concentrations: A mesocosm experiment. *Aquat. Microb. Ecol.* **34,** 93–104 (2004).
12. Von Smochulowski, M. Versuch einer mathematischen Theorie der Koagulationskinetic von Kolloidteilchen. *Z. Phys. Chem.* **92,** 129–168 (1917).
13. Ziff, R. M. & Stell, G. Kinetics of polymer gelation. *J. Chem. Phys.* **73,** 3492–3499 (1980).
14. Ruiz, J., Prieto, L. & Ortegon, F. Diatom aggregate formation and fluxes, a modeling analysis under different size-resolution schemes and with empirically determined aggregation kernels. *Deep-Sea Res. I* **49,** 495–515 (2002).
15. Geider, R. J., MacIntyre, H. L., Graziano, L. M. & McKay, R. M. L. Responses of the photosynthetic apparatus of *Dunaliella tertiolecta* (Chlorophyceae) to nitrogen and phosphorus limitation. *Eur. J. Phycol.* **33,** 5315–5332 (1998).
16. Carlson, C. A. in *Biogeochemistry of Marine Dissolved Organic Matter* (eds Hansell, D. A. & Carlson, C.) 59–90 (Academic, Amsterdam, 2002).
17. Nielsen, M. V. Growth, dark respiration and photosynthetic parameters of the coccolithophorid *Emiliania huxleyi* (Prymnesiophyceae) acclimated to different day length–irradiance combinations. *J. Phycol.* **33,** 818–822 (1997).
18. Amon, R. M. W. & Benner, R. Rapid cycling of high-molecular-weight dissolved organic matter in the ocean. *Nature* **369,** 549–552 (1994).
19. Benner, R. in *Biogeochemistry of Marine Dissolved Organic Matter* (eds Hansell, D. A. & Carlson, C.) 59–90 (Academic, Amsterdam, 2002).
20. Del Giorgio, P. A. & Duarte, C. M. Respiration in the open ocean. *Nature* **420,** 379–384 (2002).
21. Pakulski, J. D. & Benner, R. Abundance and distribution of carbohydrates in the ocean. *Limnol. Oceanogr.* **39,** 930–940 (1994).
22. Biddanda, B. & Benner, R. Carbon, nitrogen, and carbohydrate fluxes during the production of particulate and dissolved organic matter by marine phytoplankton. *Limnol. Oceanogr.* **42,** 506–518 (1997).
23. Baines, S. B. & Pace, M. L. The production of dissolved organic matter by phytoplankton and its importance to bacteria, patterns across marine and freshwater systems. *Limnol. Oceanogr.* **36,** 1078–1090 (1991).
24. Myklestad, S. M., Skånoy, E. & Hestmann, S. A sensitive and rapid method for analysis of dissolved mono- and polysaccharides in seawater. *Mar. Chem.* **56,** 279–286 (1997).
25. Wu, J., Boyle, E., Sunda, W. & Wen, L.-S. Soluble and colloidal iron in the oligotrophic North Atlantic and North Pacific. *Science* **293,** 847–849 (2001).
26. Passow, U. & Alldredge, A. L. A dye-binding assay for the spectrophotometric measurement of transparent exopolymer particles (TEP) in the ocean. *Limnol. Oceanogr.* **40,** 1326–1335 (1995).
27. Porter, K. G. & Feig, T. S. The use of DAPI for identifying and counting aquatic microflora. *Limnol. Oceanogr.* **25,** 943–948 (1980).
28. Wells, M. L. & Goldberg, E. D. Marine submicron particles. *Mar. Chem.* **40,** 5–18 (1992).
29. Mari, X. Carbon content and C:N ratio of transparent exopolymer particles (TEP) produced by bubbling of exudates of diatoms. *Mar. Ecol. Prog. Ser.* **33,** 59–71 (1999).
30. Mc Cave, I. N. Size spectra and aggregation of suspended particles in the deep ocean. *Deep-Sea Res.* **31,** 329–352 (1984).

Acknowledgements We thank A. Terbrüggen for technical assistance and M. Schartau for discussions. This work was supported by the Large-Scale Facility of the University of Bergen, Norway and the European Commission Human Potential Programme.

Competing interests statement The authors declare that they have no competing financial interests.

Correspondence and requests for materials should be addressed to A.E. (anja.engel@stonybrook.edu) or S.T. (sthoms@awi-bremerhaven.de).

Maturation trends indicative of rapid evolution preceded the collapse of northern cod

Esben M. Olsen[1]*, Mikko Heino[1,2], George R. Lilly[3], M. Joanne Morgan[3], John Brattey[3], Bruno Ernande[1] & Ulf Dieckmann[1]

[1]*Adaptive Dynamics Network, International Institute for Applied Systems Analysis, A-2361 Laxenburg, Austria*
[2]*Institute of Marine Research, P.O. Box 1870 Nordnes, N-5817 Bergen, Norway*
[3]*Northwest Atlantic Fisheries Centre, Department of Fisheries and Oceans, P.O. Box 5667, St John's, Newfoundland, Canada A1C 5X1*

* Present address: Division of Marine Biology and Limnology, Department of Biology, University of Oslo, P.O. Box 1064, Blindern, N-0316 Oslo, Norway

Northern cod, comprising populations of Atlantic cod (*Gadus morhua*) off southern Labrador and eastern Newfoundland, supported major fisheries for hundreds of years[1]. But in the late 1980s and early 1990s, northern cod underwent one of the worst collapses in the history of fisheries[2–4]. The Canadian government closed the directed fishing for northern cod in July 1992, but even after a decade-long offshore moratorium, population sizes remain historically low[4]. Here we show that, up until the moratorium, the life history of northern cod continually shifted towards maturation at earlier ages and smaller sizes.